

A scalable system to measure contrail formation on a per-flight basis

Scott Geraedts,^{*,†} Erica Brand,[†] Thomas R. Dean,[‡] Sebastian Eastham,[¶]
 Zebediah Engberg,[‡] Ulrike Hager,[†] Ian Langmore,[†] Kevin McCloskey,[†] Joe
 Yue-Hei Ng,[†] John C. Platt,[†] Tharun Sankar,[†] Aaron Sarna,[†] Marc Shapiro,[‡]
 and Nita Goyal[†]

[†]*Google, Mountain View, California*

[‡]*Breakthrough Energy, Kirkland, Washington*

[¶]*Laboratory for Aviation and the Environment, Massachusetts Institute of Technology*

E-mail: geraedts@google.com

Abstract

Persistent contrails make up a large fraction of aviation’s contribution to global warming. We describe a scalable, automated detection and matching (ADM) system to determine from satellite data whether a flight has made a persistent contrail. The ADM system compares flight segments to contrails detected by a computer vision algorithm running on images from the GOES-16 Advanced Baseline Imager. We develop a ‘flight matching’ algorithm and use it to label each flight segment as a ‘match’ or ‘non-match’. We perform this analysis on 1.6 million flight segments. The result is an analysis of which flights make persistent contrails several orders of magnitude larger than any previous work. We assess the agreement between our labels and available prediction models based on weather forecasts. Shifting air traffic to avoid regions of contrail formation has been proposed as a possible mitigation with the potential for very low

cost/ton-CO₂e. Our findings suggest that imperfections in these prediction models increase this cost/ton by about an order of magnitude. Contrail avoidance is a cost-effective climate change mitigation even with this factor taken into account, but our results quantify the need for more accurate contrail prediction methods and establish a benchmark for future development.

Introduction

Persistent contrails are cirrus clouds formed by aircraft as they fly through the upper atmosphere. Like all cirrus clouds, this ‘aviation-induced cirrus’ both blocks outgoing long-wave infrared radiation and reflects incoming short-wave radiation.^{1,2} Over the past several years, the atmospheric science community has realized that the net effect on the radiative balance of the planet is warming, by some measures more than the warming due to the carbon dioxide emissions of the aviation industry.²⁻⁷ Aircraft only form persistent (i.e. lasting longer than a few minutes) contrails when flying through pockets of air that are cold and have relative humidity greater than 100% with respect to ice, so-called ice supersaturated regions (ISSR). ISSR are relatively rare and small, so the flight trajectory changes needed to avoid contrail formation are also small.⁸⁻¹⁰ Therefore, adopting a ‘contrail avoidance’ approach of avoiding flying through ISSR could significantly reduce the warming impact of the aviation industry at potentially small cost. This is one of the most cost-effective climate change mitigations available.¹¹

Evaluating the effectiveness of contrail avoidance is difficult without empirical observation. Observing enough contrails to do large-scale evaluation was previously a difficult problem, but the development of contrail detection machine learning models based on satellite imagery^{12,13} has made it possible to automatically observe very large numbers of contrails with much higher accuracy than earlier approaches.

In this work we use historical infrared images from the GOES-16 geostationary satellite to detect persistent contrails. Based on the distance between these contrails and recorded

flight paths, we classify all flights as either making or not making contrails. Our method is fully automated and can be scaled to assess all flights over a wide area, for example this work covers an area including the entire contiguous United States over an aggregate period of 168 hours. We analyze the properties of the observed contrails, similar to previous works^{14,15} but with orders of magnitude more data.

Contrail avoidance requires the ability to predict which flights will make contrails. There has been considerable progress on developing models that can predict contrail formation.^{10,16–19} However there has been no large-scale attempt to assess how accurately these models predict contrail formation on a per-flight basis. Multiple works^{20,21} have shown that the critically important input of humidity in the upper atmosphere is often poorly predicted by weather forecasts.

Existing efforts to assess the cost and benefits of contrail avoidance^{8–11} assume perfect contrail prediction, and though this is not a prerequisite for adopting contrail avoidance, imperfections will both decrease the benefits (since some contrails will not be predicted in advance and therefore not avoided) and increase the cost (since some flights will spend extra fuel attempting to avoid creating contrails when their original flight path would not have passed through any ISSR).

In this work we compare our observations to the output of contrail prediction models. For each flight segment, we ask the models whether or not a contrail would form, check the GOES imagery to see if an observed contrail matches the flight segment, and tally up precision and recall for each model. Though our contrail observations are not perfect, we expect that the GOES instrument, with its $2km$ resolution and sensors viewing the parts of the electromagnetic spectrum where contrails are expected to trap the most heat, should be able to detect most contrails with a strong warming impact.

Our work is the first attempt to assess, for a large number of flights and independent of modeled humidity data, whether each flight made a contrail. As such it allows us to compare the performance of different contrail prediction models and the weather data that

they use. It also allows us to estimate how imperfections on prediction models affect the cost of contrail avoidance.

Materials and Methods

Data

We start by automatically detecting contrails using computer vision methods described in Ng et al.,¹³ which uses infrared images from the GOES-16 Advanced Baseline Imager (ABI)²² as input. These images cover much of the Western hemisphere. The images have a temporal resolution of 10 minutes and a spatial resolution of approximately 2 km.

We derive flight trajectories from ground-based ADS-B data provided by FlightAware (<https://flightaware.com>). All flight paths are resampled so that there is one flight waypoint per minute. Flights are divided into 10-minute ‘flight segments’, the length of 10 minutes was chosen to yield segment sizes of $\approx 150km$, the typical flight length inside ISSR.²³ This leads to 10 waypoints total for most segments, though some segments have fewer waypoints, e.g. at the start and end of the flight and where there are gaps in ADS-B coverage. We include in our analysis all segments with at least 6 waypoints. FlightAware contains a small number of unrealistic flight trajectories. To remove these, the velocity between each pair of waypoints are computed and the flight segment is dropped if this velocity exceeds $1,234.8 km/h$. Additionally, only flight waypoints whose altitude is above 7000 meters are included since persistent contrail conditions are very rare below this altitude. Apart from these considerations we process all flight waypoints available from FlightAware.

Weather data in this work comes from the European Center for Midrange Weather Forecasts (ECWMF). We use both high-resolution (HRES) forecast and ERA5 reanalysis data.²⁴ The forecast data is obtained on a $0.1^\circ \times 0.1^\circ$ grid at ‘model’ altitude levels while the reanalysis data is obtained on a $0.25^\circ \times 0.25^\circ$ grid. In order to study the effects of vertical resolution reanalysis data is obtained on both ‘model levels’ (which have $\approx 10hPa$ resolu-

tion) and ‘pressure levels’ (which have 25-50 hPa resolution). When weather forecasts are used we use the most recent forecast that would have been available if one were actually using the forecasts to make predictions, which was initialized 0-23 hours before the time of the flight waypoint.

In this work we analyze all flights inside the region shown in Fig. 1 containing the entire contiguous USA as well as much of the rest of North America.

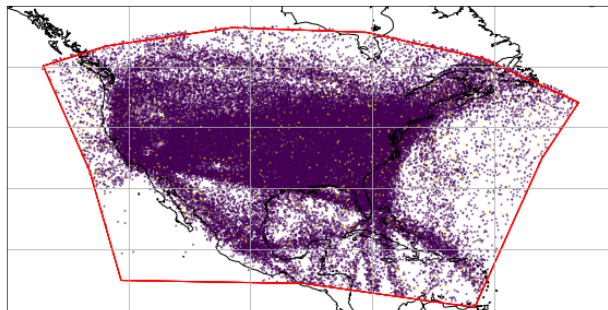


Figure 1: Illustration of the region (red) considered in this work. Each point in the figure represents one of the advected flight segments considered in this work. Yellow points correspond to segments that matched contrails while purple points correspond to segments that do not match contrails. The points in the figure represent 1% of the data considered in this work.

The data analysed in this paper comes from the time-period Apr 4 2019 – Apr 4 2020. We analyze data sampled from across a whole year to account for seasonality of contrail formation.¹² In Mar 2020 there was a large drop in air traffic density due to the COVID-19 pandemic, but we have found that quantities such as the fraction of flights matching contrails and the skill of prediction models were not meaningfully different in that month. We focus on 168 hours worth of data, distributed in 28 6-hour chunks, uniformly sampled by month and at different times of day, since this is more computationally tractable than processing an entire year.

Flight Matching algorithm

Flight matching compares, for each flight, the position of observed contrails to the position a contrail would be at if the flight had made a contrail. The expected position at the time

that the GOES ABI imaged a scene is determined through three-dimensional advection of the flight waypoints using the third-order Runge-Kutta method²⁵ and winds taken from weather data. Each waypoint is advected for two hours, covering the next 11 GOES images (10 minute time-steps). Because ice crystals in a contrail fall over time, we also sink the waypoints vertically. The crystals fall at terminal velocity, assuming a crystal size obtained by performing a quadratic fit to the distribution of ice crystal sizes given by CoCiP.¹⁶ The resulting function for radius r is:

$$r = \frac{e^{3.24+0.58 \log(t)+0.12 \log(t)^2}}{10^{-6}}. \quad (1)$$

Where r is in μm and t is in hours. We also descend the waypoints by $50m$ at the start of advection to account for wake vortex downwash. The value of $50m$ is similar to the values quoted used for the initial sinking in CoCiP.¹⁶ We next assess whether the expected location of each flight is close to any observed contrails, using a method adapted from Duda et al.¹⁴ Given a contrail detected by our computer vision algorithm, we rotate the contrail and the advected flight path to a rotated coordinate system indexed by the coordinates v and w . In this coordinate system the contrail runs from $v = -L/2$ to $v = L/2$, with L being the length of the contrail, and has $w = 0$. The advected flight waypoints have coordinates (w_i, v_i) . We consider advected flight waypoints that overlap with the contrail (between $v = -L/2 - \Delta$ and $v = L/2 + \Delta$, with $\Delta = \sqrt{C_{\text{shift}} + C_{\text{fit}}}$). The flight and the contrail match only if there are at least two overlapping waypoints.

We then find another coordinate transformation

$$\begin{aligned} w &\rightarrow (w + W) \cos(\theta) + (v + V) \sin(\theta) \\ v &\rightarrow (v + V) \cos(\theta) - (w + W) \sin(\theta), \end{aligned}$$

i.e. we shift the coordinates by (W, V) and also rotate by the angle θ . The coordinate

transformation minimizes the cost function:

$$\begin{aligned} \text{match error} = & [C_{\text{fit}} \frac{1}{N} \sum_{i=1}^N w_i^2 + C_{\text{shift}}(V^2 + W^2) \\ & + C_{\text{angle}}(1 - \cos(\theta)) + C_{\text{age}}]. \end{aligned} \quad (2)$$

A low match error indicates a good match. In other words, we shift and rotate the coordinates to find a coordinate system where the advected flight waypoints line up exactly with the contrail. The ‘fit’ term quantifies how successful we were at doing this, while the ‘shift’ and ‘angle’ quantify how big a shift and rotation is required in order to get the waypoints and the contrail to line up. A big shift and/or rotation implies that the advected flight and contrail weren’t that close to begin with, and this leads to a high match error.

The C_{fit} term represents residual ‘linearity’ error - advected flight waypoints that are not themselves linear are unlikely to have created a linear contrail. Our flight matching therefore penalizes curved flight trajectories, and in fact 0.03% of flight segments are so non-linear that this term will prevent them from matching any contrail.

The C_{shift} term is dominated by the uncertainty in the wind. If this wind is incorrect, the correct flight may advect to the wrong location, and these errors get larger the longer we advect for. We compare the wind forecast data used for advection with the wind data produced by the Mode-S data broadcast by airplanes.²⁶ The Mode-S system uses flight transponders and ground-based radar to obtain the wind velocity for selected aircraft with a high degree of accuracy. Mode-S data was obtained from FlightAware for 326,000 waypoints over the contiguous United States on Aug 20, 2021. We found a mean error of 11 km/h.

The C_{angle} term is dominated by the difference in wind errors at different locations, which will rotate the advected flight path. For the same waypoints as used in the C_{shift} analysis, we compared the wind speeds at two locations separated by the length of our typical segment (150 km), finding a mean error of 3.8 degrees/hour.

The constants C_{fit} , C_{shift} and C_{angle} were chosen so that each term should be ≈ 1 when

the error is as large as the mean error. Specifically:

$$C_{\text{fit}} = \frac{1}{(1\text{km})^2} \quad (3)$$

$$C_{\text{shift}} = \frac{1}{(10\text{km}/h \times t)^2} \quad (4)$$

$$C_{\text{angle}} = \frac{1}{1 - \cos(5 \text{ degrees}/\text{hour} \times t)} \quad (5)$$

where t is the difference between the time of the flight and the time the contrail was observed, in hours. Since a typical error will lead to each term in Eq. (2) being 1, a flight is labeled a match if the overall match error is ≤ 3 .

The C_{age} term is a correction factor for the C_{shift} and C_{angle} terms which become increasingly permissive as a contrail gets older. It was tuned by a small grid search after the other terms had been selected, to yield an age distribution of contrails similar to what has been found in previous observation studies, in particular Figure 6 of Vazquez-Navarro et al.¹⁵

$$C_{\text{age}} = t \quad (6)$$

Additionally, we have attempted to handle the case where multiple flights match what appears to be the same contrail. In general when this happens we call both flights a match, unless one of the matching flights is much better than the other (specifically, the difference in match errors ≥ 1). In that case the worse matching flight is not counted as matching that contrail (it can still match other contrails).

Matching individual segments to contrails leads to problems when contrails overlap the segment boundaries. Therefore during flight matching we match contrails to entire flights, and if a match is found label all segments that overlap the contrail as matches. A pseudocode version of the algorithm is given in Algorithm 1.

To assess the performance of flight matching we created a tool that displays sequences of images similar to Fig. 2. Each image contains the flight segment in question, all other nearby


```

SegmentMatches[all segments]  $\leftarrow$  False
for Flight in AllFlights do
    for Contrail in AllContrails do
        | Scores[Flight,Contrail]  $\leftarrow$  GetScore(Flight, Contrail)
for Flight in AllFlights do
    for Contrail in AllContrails do
        if Scores[Flight,Contrail] > 3 then
            | continue
        BetterMatchFound  $\leftarrow$  False
        for OtherFlight in AllFlights do
            | if Scores[Flight,Contrail] - Scores[OtherFlight,Contrail] > 1 then
            | | BetterMatchFound  $\leftarrow$  True
        if not BetterMatchFound then
            for Segment in GetSegments(Flight) do
                if Overlaps(Segment, Contrail) then
                    | SegmentMatches[Segment]  $\leftarrow$  True

```

Algorithm 1: Pseudocode for flight matching algorithm

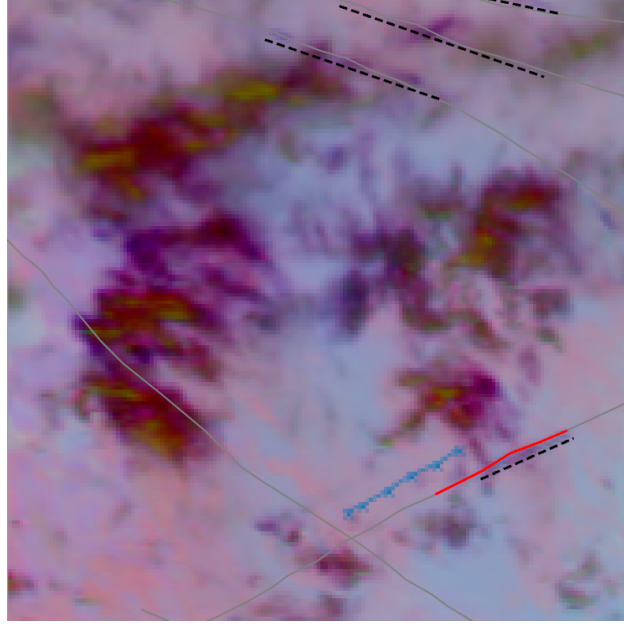


Figure 2: An example of our ADM system. The dashed black lines indicate linearized contrails from our computer vision model. The red line indicates the advected flight path at the time the satellite image was taken and the blue line is the original flight path. We compare the red line with all black lines, and determine whether we think the flight segment in question matches a contrail (in this case, the result is that it does). The gray lines are all the advected flight paths that pass through the image.

flights, a false-color GOES infrared image, and detected contrails. We randomly selected 1000 flight segments from our dataset and three authors of this work assessed whether the flight segment matched a contrail, with a majority vote among the humans determining the correct label. We found that 88% of the flights that the humans thought matched contrails were also labeled as matches by our automated matching. Only 50% of the flights labeled as matches by the automated matching were labeled as matches by the humans. Most of the errors come from cases where there are a large number of flights, and multiple flights that are near the same contrail. The humans were able to uniquely determine which flight matched the contrail, while our automated matching was more likely to match all nearby flights to the same contrail. In the results section we study how the errors in the automated matching affect its results by showing results for both the automated matching and the data with human-evaluated flight matches.

Prediction models

We predict whether each flight segment will make a contrail using the methods described below. In the Results section we assess whether these predictions agree with our observations.

Baseline

The minimum requirements for persistent contrail formation are that the Schmidt-Appleman criterion (SAC)^{27–29} is satisfied and the relative humidity over ice (RHi) is greater than 100%.³⁰ The ‘Baseline’ model evaluated in this work makes predictions solely based on these requirements. In order to account for subgrid scale variations and biases of RHi in weather forecast data, when predicting contrails it is common to apply a threshold for RHi different from 100%, or to rescale the data.^{10,16,31,32} To account for this we experiment with varying the RHi threshold when displaying results. When making predictions for an entire flight segment consisting of multiple waypoints, we average the RHi and binary SAC values before comparing them to the threshold (other ways of aggregating give similar or worse results).

When computing SAC we assume an aircraft engine efficiency of 0.3 for all aircraft,³³ though trying other values (0.2, 0.4) does not have a noticeable effect.

For predicting contrail formation, weather variables are linearly interpolated from gridded historical weather data. RH_i is computed from specific humidity which was logarithmically interpolated in altitude to handle its large variations. We show results for both forecast and reanalysis weather data. The Baseline model only considers the weather at the flight waypoint timestamp.

CoCiP

The Contrail Cirrus Prediction model (CoCiP)^{16,17} is a widely-used parameterized physics model of contrail evolution. After determining that a contrail will form and persist, CoCiP models contrail lifetime through initial downdraft, advection and fall, continually reassessing whether the contrail persists or sublimates. Modeling the microphysical properties of the contrail allows CoCiP to predict quantities such as optical depth and radiative forcing. It also suggests that CoCiP may be better than the Baseline at predicting whether contrails will persist long enough to be visible in GOES. Our approach makes it possible to assess this question empirically.

The geostationary images in this work have a resolution of 2 *km* and so cannot see all small or faint contrails, or contrails obscured by other clouds. Though the climate impact of such contrails may be small, in order to assess how weather data errors affect prediction models, it is best to compare our observations to only contrails that CoCiP predicts should be visible in GOES. Though CoCiP does not predict GOES visibility directly there are a few quantities we could use as a proxy. For example, CoCiP predicts how long each contrail will persist, and contrails that persist longer will have a chance to appear in more GOES images. One drawback of using contrail persistence time as a proxy for observability is that does not account for small or faint contrails. A better proxy might therefore be the product of optical depth and width, integrated over contrail lifetime. Even this doesn't capture the case where

CoCiP predicts that a contrail will be difficult to observe because of other clouds above or below it. The proxy for observability we use is the integral of the predicted radiative forcing of the contrail in the long wave infrared, for the times for which we are making observations. Much like RHi in the Baseline model, we average this ‘long-wave energy forcing’ LWEF across segments and show results for different thresholds. LWEF is the quantity most similar to how different the contrail pixels in GOES images are from the surrounding pixels.

We obtain CoCiP predictions through the API made available by Breakthrough Energy at <https://api.contrails.org>, which implements the original CoCiP algorithm along with modifications developed in.^{5,9,10,34}

Metrics

We define ‘precision’ as the fraction of predicted flight segments which are considered to match a contrail using our method, and ‘recall’ as the fraction of matched contrails which are successfully predicted. A prediction model which always agrees with our observations would have precision=1 and recall=1.

The precision and recall of a given model depends on what threshold of relative humidity (or LWEF for CoCiP) is used. A high threshold can avoid predicting observed contrails that aren’t there, but at the cost of potentially missing some observed contrails (high precision, low recall), while a low threshold will correctly find most observed contrails but also potentially predict that some flights will make contrails when no contrail is observed (high recall, low precision). Which threshold is appropriate depends on the application. We compute results for multiple different thresholds to show all the different results that different thresholds can produce.

Previous works^{9,11} have compared the climate benefits of avoiding contrails with the cost of the extra fuel needed to do the avoidance. They assume a perfect contrail prediction model, but imperfections in prediction models will change the cost/benefit analysis. Roughly speaking, the benefit needs to be multiplied by the recall, because some contrails are never

predicted by the model and never avoided. The cost also needs to be increased by $1/\text{precision}$, because some flights are rerouted (using extra fuel) for no benefit. In total the cost/benefit reduction factor (CBRF) is $1/(\text{precision} \times \text{recall})$. This CBRF is an estimate only since its exact value depends on the details of contrail avoidance.

Results and Discussion

Properties of observed flight matches

In this work we analyze using our automated detection and matching (ADM) system 255,341 flights, broken into ~ 1.8 million flight segments. We find that 3.5% of flight segments in FlightAware are observed to match a contrail, and 14.5% of flights have at least one segment that matches a contrail.

When contrails initially form they $\approx 100m$ in width¹⁶ which makes them difficult to see in infrared GOES images which have have 2 *km* resolution at nadir. Wind shear and diffusion spread the contrail out as it ages.¹⁶ The age of each contrail when it is first observed is shown in Fig. 3. Most flight segments start matching contrails about half an hour after formation, with the mean time until first observation being 41 minutes, approximately consistent with existing literature.^{14,15,35} There are likely many flight segments that make contrails which sublime before they are large enough to be seen in GOES. We label those flight segments non-matches since we never detect those contrails. This is acceptable since such contrails have only a small climate impact.

Fig. 3 also shows the effect of incorporating time (as in Eq. 6) in the flight matching algorithm, which prevents some very old flight segments from matching contrails. With or without the C_{age} term, the number of contrails with initial detection age more than two hours is small, which motivates our decision to only compare flights to contrails detected in the first two hours after the flight. It is possible that a contrail could spread out so slowly that it is only large enough to be detected (and therefore matched) after two hours, in which

case we would miss that match in this work. We have not found any examples of this in our data.

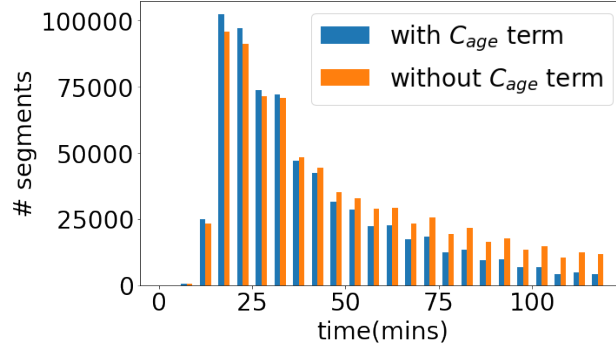


Figure 3: Histogram of the age of each flight segment at the first time it matches a contrail.

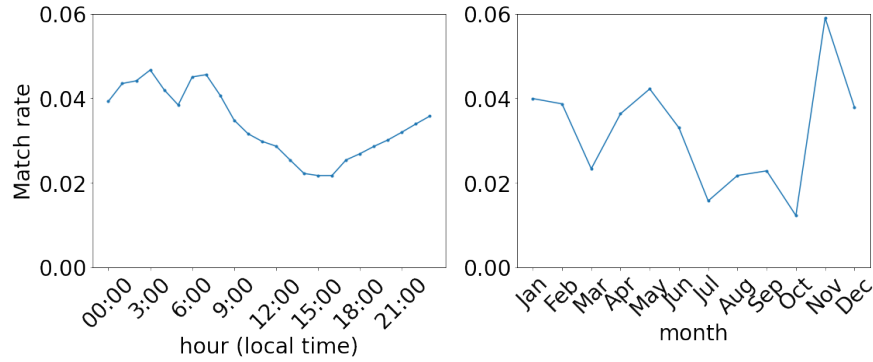


Figure 4: Match rate (fraction of flight segments observed to match a contrail) as a function of time of day(left), and time of year (right)

Figure 4 shows the match rate (the fraction of flight segments the ADM system matches to a contrail) as a function of local time of day and time of year. The results seem to show a diurnal cycle with a higher fraction of flight segments being matched to contrails in the night and morning, and a lower fraction in the afternoon. This is consistent with previous works^{12,36–38} which also found fewer contrails in the afternoon. We see a large amount of variation from month to month. This is likely because we are only looking at 2-3 days for each month, so the number of different weather systems we sample is not very large. Previous work^{12,14,37,39} has suggested that fewer contrails form in the summer months, which appears to be supported by our data. To avoid creating correlations between time of day and time of year, the results in Fig. 4 use 28 24-hour chunks (rather than 6 hour chunks).

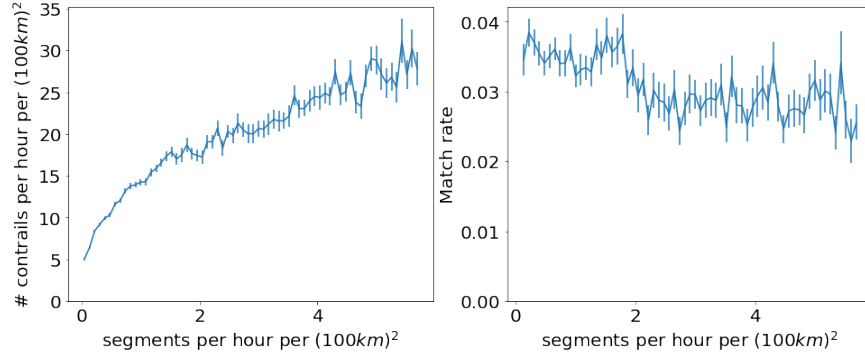


Figure 5: Number of contrails (left) and match rate (right) as a function of flight segment density. Fewer contrails are detected and matched at high flight densities. Error bars are one standard deviation, obtained by bootstrapping (resampling with replacement)

In Fig. 5 we study the dependence of our results on flight density. We divide our region into $(1^\circ \text{ latitude}) \times (1^\circ \text{ longitude}) \times (1 \text{ hour})$ boxes, and compute the number of flights, contrails, and matches in each box. We then add together all the bins with similar numbers of flight segments, and compute the overall number of contrails detected and match rate. The result is a breakdown of our dataset by flight density. One might expect that the number of contrails detected would grow linearly with the number of flights, but instead in the left panel of Fig. 5 we see that the growth seems to slow down at around 5 flight segments per bin. Similarly one might expect the match rate to be constant with flight density but it seems to drop by 20% at high flight densities. In summary we detect fewer contrails than expected at high flight density, and consequently fewer of the flights at high flight density end up matching contrails. One explanation for this is that contrails are harder to detect when there are many of them overlapping, as suggested by Minnis et al.³⁸ There may also be a physical explanation, for example in areas of high flight density there may not be enough excess water vapor available for all flights to make contrails.⁵

Comparison with prediction models

We now compare our detection results to various prediction models. To illustrate our method, let us first consider the example of the Baseline model with HRES forecast weather data, and

assuming that all flights with $\text{RHi} > 95\%$ are predicted to make a contrail. The confusion matrix for this case is given in Table 1. The results show that only a third of the contrails we observe are predicted, and no contrail is observed for 85% of the segments which are predicted to make a contrail.

Table 1: Confusion matrix for the forecast Baseline model with an $\text{RHi} > 95\%$ cutoff.

	Detected	Not detected
Predicted	20,877	116,435
Not predicted	43,024	1,662,780
Precision	0.15	
Recall	0.33	

As discussed above, the threshold of humidity 95% is not the only possibility. We repeat the above study for different thresholds from 70 – 110%, and plot all the precision/recall results as points on a curve in Fig. 6. We then do the same thing for the Baseline model with ERA5 reanalysis weather data defined on ‘model’ vertical levels ($\text{ERA5}_{\text{model}}$), and again for the Baseline Model with ERA5 data on ‘pressure’ levels ($\text{ERA5}_{\text{pressure}}$), and the CoCiP model using HRES forecast data. In the CoCiP case we threshold on LWEF rather than RHi , and use thresholds 20,000 – 500,000 J/m . We have also computed the performance of the CoCiP model using ERA5 reanalysis inputs, the results (not shown) were very similar to the Baseline model using reanalysis inputs.

Comparing the different prediction models, the Baseline model based $\text{ERA5}_{\text{pressure}}$ performs the worst. For example with a 95% RHi threshold the model achieves precision 0.14, recall 0.25. This is not surprising: ISSRs are vertically thin and so it is not unexpected that a model with poor vertical resolution should have a hard time predicting them. The remaining models all give very similar performance. In particular the reanalysis and forecast data have very similar results when they both use the same vertical resolution.

The performance of CoCiP and the Baseline model were very similar when both used the same weather as input. In the plot we show CoCiP using LWEF as a proxy for whether we can detect a contrail. Using CoCiP predictions of lifetime or optical depth instead gives

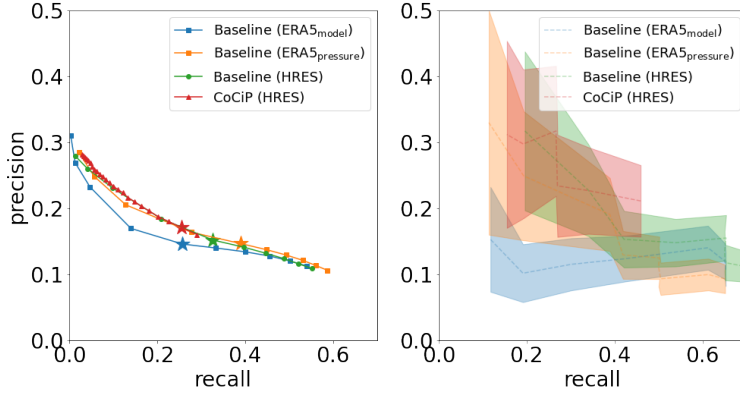


Figure 6: (Left) Precision/recall for the prediction models studied in this work, using our ADM system. We trace out curves by trying multiple different thresholds as described in the text. For Baseline models the starred points correspond to a threshold of 95% RH_i, and each other point results from adjusting the threshold by 5 percentage points. CoCiP is similar but with 40,000 J/m for the starred point and steps of 20,000 J/m . (Right) Precision/recall when comparing predictions to human flight matching results instead of automated matching. The prediction models agree better with the human labels, though the results are much noisier due to small sample sizes. Error bars represent one standard deviation computed using bootstrapping with 1000 samples.

worse agreement with our observations. This suggests that the primary source of error in contrail forecasts comes from inaccurate RH_i available from weather data. Microphysical modeling is useful to determine properties of contrails (such as radiative forcing) when RH_i data is accurate, but we find no evidence that it improves predictions of whether contrails will be observed.

In these results we use the forecast wind data for advection, using reanalysis wind data the quantitative results are very similar and the relative ordering of the different weather models are unchanged.

The results above compare prediction models to observations, but our observations are not perfect. We now attempt to quantify the impact of these imperfections on the results in Fig. 6.

The performance of the ADM system in Ng et al.¹³ was evaluated relative to human-generated labels. It was found to miss 30% of contrails and 30% of the objects it recognized as contrails were in fact false positives. Errors of the contrail detector may lead to errors

in the ADM system, or they may not, e.g. if the detector incorrectly detects a contrail that is far from any flight paths, then no flight segment will be affected. This makes it difficult to exactly quantify the impact of contrail detection errors on our results, but due to such errors, even a perfect prediction model would achieve a maximum precision/recall in Fig. 6 around 0.7.

To quantify the effects of automated flight matching errors on our results, in Fig. 6 we also compute precision and recall for our prediction models using only the flight segments with human-evaluated matching obtained above. Since for the human labeled data we have only 1000 flight segments (of which 29 were labeled by humans as matching contrails), the statistical error bars are much larger. To quantify this we ‘bootstrap’ by resampling the data with replacement, the resulting error bars are indicated by the shaded regions in Fig. 6. The results allow us to quantify how much an improved flight matching algorithm could improve the agreement between prediction models and our observations. We see that though the agreement is improved substantially the observed precision and recall falls well short of what a perfect prediction model could achieve. This is consistent with existing literature, for example Gierens et al.²⁰ compared ERA5 reanalysis to aircraft based MOZAIC measurements and found 16% precision and 21% recall when assessing whether $RH_i > 100\%$, while Agarwal et al.²¹ compared ERA5 measurements to radiosonde data and found that ERA5 incorrectly predicted the conditions for persistent contrail formation 87% of the time.

Implications for contrail avoidance

In the example above of the forecast Baseline model with a 95% RH_i threshold, if contrail avoidance were attempted the number of flights segments we observe making contrails would be reduced by 33%, and of the flight whose flight paths were changed to avoid contrails, 85% would not have matched a contrail even if they were not rerouted. This implies a CBRF of $1/(0.15 \times 0.33) \approx 20$. We can decrease the CBRF by choosing a better threshold, and it is possible to find a threshold where it is ≈ 16 for all models. Furthermore we know that

imperfections in our ADM system are artificially inflating the CBRF. If instead we used the mean values of the bootstrapped human labels as a guide, the CBRF is 8 – 13.

Discussion

In this work we have matched a large number flights over a wide area to observed contrails. Our method can be used to generate large datasets of contrails for further analysis, and could become the basis for a system of verifying contrail avoidance.

Our results establish a benchmark for the performance on contrail prediction models while we hope aid in improving those models. An important step would be to forecasts of relative humidity at high altitudes. Alternatively, it may be possible to use our data to analyze and correct for possible biases in weather forecast data, or to use real-time observations of contrails to predict future contrail formation. Our method provides a way to measure whether approaches like these actually improve prediction accuracy.

The values of the CBRF quoted above may also be artificially high due to errors in our detection model. Other factors (such as the cost of mistakenly diverting aircraft *into* contrail formation regions) are also not considered here. A more detailed estimation of the CBRF would be a useful direction for future work. Caldiera et al.¹¹ reports that contrail avoidance has benefits 1000 times larger than its cost, so even with the CBRF reported here contrail avoidance using current technology is likely a high value climate change mitigation strategy.

Further improvements to the ADM system described here are possible. Improvements to contrail detection are discussed in Ng et al.¹³ The flight matching procedure can also be improved, especially in high flight density areas. A more detailed treatment of the case where multiple flights match the same contrail is desirable but difficult. An improved ground-truth flight-matching dataset would enable future progress. Additional data inputs to flight matching algorithms could improve their accuracy: e.g., contrail altitude estimates could be compared to flight altitudes. Cloud top height can be extracted from geostationary images,⁴⁰ but such models suffer from poor performance for thin clouds⁴¹ so the models

should be validated against contrails specifically to determine whether they are appropriate for this use case. Dealing with non-linear contrails and flight trajectories is another area for further improvement. This work’s flight matching algorithm also treats each detected contrail independently, but contrails appearing near each other in consecutive frames are likely the same contrail, and could be required to match the same flight segment, as done recently in Chevallier et al.³⁵ A dataset of tracked contrails, such as created on a small scale in Vazquez-Navarro et al.,⁴² could lead to further improvement.

This work provides an empirical method to assess whether a flight made a persistent contrail, but not all persistent contrails produce the same amount of warming. A useful extension of this work would be to observe the radiative forcing of each contrail and compare that to predictions.

This work establishes an empirical basis for evaluation of contrail avoidance strategies, beginning with the continental United States. The techniques which we demonstrate using the GOES-16 satellite can be readily extended to cover any area of the world with sufficiently high-resolution geostationary satellite coverage.

The dataset used to generate the results in this work is available at https://storage.googleapis.com/contrails_measurement_paper_data/dataset.parquet.gzip.

Acknowledgement

The authors thank Christopher Van Arsdale, Vincent Meijer, Maria Barbosa and Louis Robion for useful discussions, Anna Michalek for feedback on the manuscript, Ethan Koenig for contributions to our codebase and Alex Merosé, Aaron Bell and the Google Anthromet team for helping to provide weather data. Dr. Eastham’s participation in this research was partially supported by the U.S. Federal Aviation Administration Office of Environment and Energy through ASCENT, the FAA Center of Excellence for Alternative Jet Fuels and the Environment, Project 78 through FAA Award Number 13-C-AJFE-MIT under the

supervision of Nicole Didyk-Wells. Any opinions, findings, conclusions or recommendations expressed in this material are those of the authors and do not necessarily reflect the views of the FAA.

References

- (1) Myhre, G.; Stordal, F. On the tradeoff of the solar and thermal infrared impact of contrails. *Geophys. Res. Lett.* **2001**, *28*, 3119–3122.
- (2) Burkhardt, U.; Karcher, B. Global radiative forcing from contrail cirrus. *Nature Climate Change* **2011**, *1*, 54–58.
- (3) Bock, L.; Burkhardt, U. Reassessing properties and radiative forcing of contrail cirrus using a climate model. *Journal of Geophysical Research: Atmospheres* **2016**, *121*, 9717–9736.
- (4) Chen, C.-C.; Gettelman, A. Simulated radiative forcing from contrails and contrail cirrus. *Atmospheric Chemistry and Physics* **2013**, *13*, 12525–12536.
- (5) Schumann, U.; Penner, J. E.; Chen, Y.; Zhou, C.; Graf, K. Dehydration effects from contrails in a coupled contrail–climate model. *Atmospheric Chemistry and Physics* **2015**, *15*, 11179–11199.
- (6) Bickel, M.; Ponater, M.; Bock, L.; Burkhardt, U.; Reineke, S. Estimating the effective radiative forcing of contrail cirrus. *Journal of Climate* **2020**, *33*, 1991–2005.
- (7) Lee, D. S.; Fahey, D.; Skowron, A.; Allen, M.; Burkhardt, U.; Chen, Q.; Doherty, S.; Freeman, S.; Forster, P.; Fuglestvedt, J.; others The contribution of global aviation to anthropogenic climate forcing for 2000 to 2018. *Atmospheric Environment* **2021**, *244*, 117834.
- (8) Avila, D.; Sherry, L.; Thompson, T. Reducing global warming by airline contrail avoidance: A case study of annual benefits for the contiguous United States. *Transportation Research Interdisciplinary Perspectives* **2019**, *2*, 100033.

- (9) Teoh, R.; Schumann, U.; Majumdar, A.; Stettler, M. E. Mitigating the climate forcing of aircraft contrails by small-scale diversions and technology adoption. *Environmental Science & Technology* **2020**, *54*, 2941–2950.
- (10) Teoh, R.; Schumann, U.; Gryspeerdt, E.; Shapiro, M.; Molloy, J.; Koudis, G.; Voigt, C.; Stettler, M. E. J. Aviation contrail climate effects in the North Atlantic from 2016 to 2021. *Atmospheric Chemistry and Physics* **2022**, *22*, 10919–10935.
- (11) Caldeira, K.; McKay, I. Contrails: tweaking flight altitude could be a climate win. *Nature* **2021**, *593*, 341–341.
- (12) Meijer, V. R.; Kulik, L.; Eastham, S. D.; Allroggen, F.; Speth, R. L.; Karaman, S.; Barrett, S. R. Contrail coverage over the United States before and during the COVID-19 pandemic. *Environmental Research Letters* **2022**, *17*, 034039.
- (13) Ng, J. Y.-H.; McCloskey, K.; Cui, J.; Meijer, V. R.; Brand, E.; Sarna, A.; Goyal, N.; Arsdale, C. V.; Geraedts, S. OpenContrails: Benchmarking Contrail Detection on GOES-16 ABI. 2023.
- (14) Duda, D. P.; Minnis, P.; Nguyen, L.; Palikonda, R. A Case Study of the Development of Contrail Clusters over the Great Lakes. *Journal of the Atmospheric Sciences* **2004**, *61*, 1132–1146.
- (15) Vázquez-Navarro, M.; Mannstein, H.; Kox, S. Contrail life cycle and properties from 1 year of MSG/SEVIRI rapid-scan images. *Atmospheric Chemistry and Physics* **2015**, *15*, 8739–8749.
- (16) Schumann, U. A contrail cirrus prediction model. *Geoscientific Model Development* **2012**, *5*, 543–580.
- (17) Schumann, U.; Mayer, B.; Graf, K.; Mannstein, H. A Parametric Radiative Forcing Model for Contrail Cirrus. *Journal of Applied Meteorology and Climatology* **2012**, *51*, 1391 – 1406.
- (18) Fritz, T. M.; Eastham, S. D.; Speth, R. L.; Barrett, S. R. H. The role of plume-scale processes in long-term impacts of aircraft emissions. *Atmospheric Chemistry and Physics* **2020**, *20*, 5697–5727.

- (19) Yin, F.; Grewe, V.; Castino, F.; Rao, P.; Matthes, S.; Dahlmann, K.; Dietmüller, S.; Frömming, C.; Yamashita, H.; Peter, P.; Klingaman, E.; Shine, K.; Lührs, B.; Linke, F. Predicting the climate impact of aviation for en-route emissions: The algorithmic climate change function submodel ACCF 1.0 of EMAC 2.53. *Geoscientific Model Development Discussions* **2022**, *2022*, 1–34.
- (20) Gierens, K.; Matthes, S.; Rohs, S. How Well Can Persistent Contrails Be Predicted? *Aerospace* **2020**, *7*.
- (21) Agarwal, A.; Meijer, V. R.; Eastham, S. D.; Speth, R. L.; Barrett, S. R. H. Reanalysis-driven simulations may overestimate persistent contrail formation by 100%–250%. *Environmental Research Letters* **2022**, *17*, 014045.
- (22) Goodman, S. J.; Schmit, T. J.; Daniels, J.; Redmon, R. J. *The GOES-R series: a new generation of geostationary environmental satellites*; Elsevier, 2019.
- (23) Gierens, K.; Spichtinger, P. On the size distribution of ice-supersaturated regions in the upper troposphere and lowermost stratosphere. *Annales Geophysicae*. 2000; pp 499–504.
- (24) Hersbach, H.; Bell, B.; Berrisford, P.; Hirahara, S.; Horányi, A.; Muñoz-Sabater, J.; Nicolas, J.; Peubey, C.; Radu, R.; Schepers, D.; others The ERA5 global reanalysis. *Quarterly Journal of the Royal Meteorological Society* **2020**, *146*, 1999–2049.
- (25) Bogacki, P.; Shampine, L. F. A 3 (2) pair of Runge-Kutta formulas. *Applied Mathematics Letters* **1989**, *2*, 321–325.
- (26) de Haan, S. High-resolution wind and temperature observations from aircraft tracked by Mode-S air traffic control radar. *Journal of Geophysical Research: Atmospheres* **2011**, *116*.
- (27) Schmidt, E. Die Entstehung von Eisnebel aus den Auspuffgasen von Flugmotoren. 1941; <https://elib.dlr.de/107948/>, Eintrag von Ulrich Schumann, zur Sicherstellung des Zugangs zu diesem wissenschaftshistorisch wichtigen Dokument; mit Zustimmung des Rechteinhabers (Nachfolger des Oldenbourg Verlags).

- (28) Appleman, H. S. The Formation of Exhaust Condensation Trails by Jet Aircraft. *Bulletin of the American Meteorological Society* **1953**, *34*, 14–20.
- (29) Schumann, U. On conditions for contrail formation from aircraft exhausts. *Meteorologische Zeitschrift* **1996**, *5*, 4–23.
- (30) Gierens, K.; Spichtinger, P.; Schumann, U. Ice supersaturation. *Atmospheric Physics: Background–Methods–Trends* **2012**, 135–150.
- (31) Schumann, U.; Poll, I.; Teoh, R.; Koelle, R.; Spinielli, E.; Molloy, J.; Koudis, G. S.; Baumann, R.; Bugliaro, L.; Stettler, M.; Voigt, C. Air traffic and contrail changes over Europe during COVID-19: a model study. *Atmospheric Chemistry and Physics* **2021**, *21*, 7429–7450.
- (32) Li, Y.; Mahnke, C.; Rohs, S.; Bundke, U.; Spelten, N.; Dekoutsidis, G.; Groß, S.; Voigt, C.; Schumann, U.; Petzold, A.; Krämer, M. Upper-tropospheric slightly ice-subsaturated regions: frequency of occurrence and statistical evidence for the appearance of contrail cirrus. *Atmospheric Chemistry and Physics* **2023**, *23*, 2251–2271.
- (33) Ponater, M.; Marquart, S.; Sausen, R. Contrails in a comprehensive global climate model: Parameterization and radiative forcing results. *Journal of Geophysical Research: Atmospheres* **2002**, *107*, ACL 2–1–ACL 2–15.
- (34) Shapiro, M.; Engberg, Z.; Teoh, R.; Stettler, M.; Dean, T.; Schemann, U.; Voigt, C. pycontrails: Python library for modeling aviation climate impacts. <https://zenodo.org/record/8160906>.
- (35) Chevallier, R.; Shapiro, M.; Engberg, Z.; Soler, M.; Delahaye, D. Linear Contrails Detection, Tracking and Matching with Aircraft Using Geostationary Satellite and Air Traffic Data. *Aerospace* **2023**, *10*.
- (36) Minnis, P.; Kirk Ayers, J.; Weaver, S. P. Surface-based observations of contrail occurrence frequency over the US, April 1993–April 1994. *4 NASA Ref. Publ.* **1997**, *1404*, 1157–1160.

- (37) Palikonda, R.; Minnis, P.; Duda, D. P.; Mannstein, H. Contrail coverage derived from 2001 AVHRR data over the continental United States of America and surrounding areas. *Meteorologische Zeitschrift* **2005**, *14*, 525–536.
- (38) Minnis, P.; Bedka, S. T.; Duda, D. P.; Bedka, K. M.; Chee, T.; Ayers, J. K.; Palikonda, R.; Spangenberg, D. A.; Khlopenkov, K. V.; Boeke, R. Linear contrail and contrail cirrus properties determined from satellite data. *Geophysical Research Letters* **2013**, *40*, 3220–3226.
- (39) Duda, D. P.; Minnis, P.; Khlopenkov, K.; Chee, T. L.; Boeke, R. Estimation of 2006 Northern Hemisphere contrail coverage using MODIS data. *Geophysical Research Letters* **2013**, *40*, 612–617.
- (40) Strandgren, J.; Bugliaro, L.; Sehnke, F.; Schröder, L. Cirrus cloud retrieval with MSG/SEVIRI using artificial neural networks. *Atmospheric Measurement Techniques* **2017**, *10*, 3547–3573.
- (41) Strandgren, J.; Fricker, J.; Bugliaro, L. Characterisation of the artificial neural network CiPS for cirrus cloud remote sensing with MSG/SEVIRI. *Atmospheric Measurement Techniques* **2017**, *10*, 4317–4339.
- (42) Vazquez-Navarro, M.; Mannstein, H.; Mayer, B. An automatic contrail tracking algorithm. *Atmospheric Measurement Techniques* **2010**, *3*, 1089–1101.